



**Mechanistic Understanding of Methane-to-Methanol
Conversion on Graphene-Stabilized Single-Atom Iron
Centers**

| | |
|-------------------------------|---|
| Journal: | <i>Catalysis Science & Technology</i> |
| Manuscript ID | CY-ART-05-2021-000826.R1 |
| Article Type: | Paper |
| Date Submitted by the Author: | 10-Jul-2021 |
| Complete List of Authors: | Hong, Sungil; University of Pittsburgh, Chemical Engineering Mpourmpakis, Giannis; University of Pittsburgh, Chemical and Petroleum Engineering |
| | |

ARTICLE

Mechanistic Understanding of Methane-to-Methanol Conversion on Graphene-Stabilized Single-Atom Iron Centers

Sungil Hong and Giannis Mpourmpakis*

Received 00th January 20xx,
Accepted 00th January 20xx

DOI: 10.1039/x0xx00000x

The functionalization of methane to value-added liquid chemicals remains as one of the “grand challenges” in chemistry. In this work, we provide insights into the direct methane-to-methanol conversion mechanisms with H_2O_2 as an oxidant on single Fe-atom centers stabilized on N-functionalized graphene, using first principles calculations. By investigating a series of different reaction paths on various active centers and calculating their turnover frequencies, we reveal that a H_2O_2 -mediated radical mechanism and a Fenton-type mechanism are energetically the most plausible pathways taking place on di- and mono-oxo centers, respectively. Due to the thermodynamic preference of the mono-oxo center formation over the di-oxo at the reaction conditions, the Fenton-type mechanism appears to determine the overall catalytic activity. On the other hand, a hydroxy(oxo) center, which is thermodynamically the most favorable center, is found to be catalytically inactive. Hence, the high activity is attributed to a fine balance of keeping the active centers as oxo-species during the reaction conditions. Moreover, we reveal that the presence of solvent (water) can accelerate or slow down different pathways with the overall turnover of the dominant Fenton-type reaction being decreased. Importantly, this work reveals the nature of active sites and a gamut of reaction mechanisms for the direct conversion of methane to methanol rationalizing experimental observations and aiding the search for room temperature catalysts of methane to liquid products.

Introduction

Methane (CH_4), the simplest hydrocarbon, is one of the most important energy sources because of its vast reserves. Natural gas is one of the most widely used fuels having generated energy of 3.8×10^{13} kWh in 2018 and is expected to reach 5.9×10^{13} kWh in 2050, accounting for 20% of primary energy consumption over the globe¹. Taking into account the presence of other methane sources (e.g., crystalline hydrates², shale gas³, and biogas⁴), which have the potential to be fully utilized with advancements in technology and infrastructure, establishes methane as an undoubtedly vital feedstock in our future energy portfolio. Nevertheless, there are technical hurdles in transporting this gaseous C_1 feedstock from remote production locations to chemical plants for its utilization and chemical conversion. Thus, developing efficient methane conversion processes to transportable liquid products is a critical issue to reduce the cost of the energy-intensive methane storage under low temperatures and high pressures⁵. In particular, methanol (CH_3OH) is an ideal target product, because it can be used as a diesel-blended fuel⁶ and in direct methanol fuel cells⁷, as well as in commercial technology to produce C_{2+} hydrocarbons⁸⁻¹⁰. The current industrial process to produce CH_3OH from CH_4 operates indirectly involving syngas production (a mixture of CO and H_2). Despite the high yields, syngas production suffers from high

cost and low energy efficiency because of the high operation temperature (> 850 °C) and large infrastructure, which limits the use of methanol in the fuel industry¹¹⁻¹⁴. Thus, many efforts have been made to discover industrially viable processes for the direct methane conversion to methanol over the past decades. However, the direct conversion is extremely challenging primarily due to the low intrinsic reactivity of CH_4 resulting from the strong C-H bonds and absence of a dipole moment, which necessitates harsh reaction conditions (e.g., high temperatures and reactive oxidative reagents)¹⁵. Unfortunately, the use of harsh conditions mostly leads to over-oxidation and/or very low selectivity to desired products, because of the higher reactivity of the latter than that of methane¹⁴⁻¹⁶. Therefore, it is of high importance to discover catalytic systems that directly convert methane to methanol under mild conditions with low energy input and high selectivity.

From the pioneering works by Staley^{17,18}, Freiser^{19,20}, Armentrout^{21,22}, Schwarz²³⁻²⁵, and Yoshizawa²⁶⁻²⁸ in 1980s and 90s, cationic transition metal oxides have been extensively investigated for C-H activation of unsaturated hydrocarbons in the gas phase, among which FeO^+ attracted particular interest. The biradical double bond of FeO^+ in the high spin ground state, which is produced from Fe^+ accepting an oxygen atom from N_2O , was revealed to be highly reactive for hydrogen abstraction from hydrocarbons^{24,26}. When methane is added as a reactant, the methyl group forms a $\text{Fe}^+\text{-C}$ bond after C-H activation and then migrates to hydroxyl to produce methanol; this reaction is characterized by two important spin inversions from sextet to quartet and back to sextet²⁶⁻²⁸. In turn, the discovery of biomimetic activity of iron complexes embedded in

Department of Chemical Engineering, University of Pittsburgh, Pittsburgh, Pennsylvania 15261, United States

*Electronic Supplementary Information (ESI) available: See DOI: 10.1039/x0xx00000x

zeolites for hydrocarbons conversion by Panov et al.^{29,30} motivated extensive research on transition metals loaded on stable and porous supports. Especially, Fe-containing MFI, BEA, CHA, and AEI type zeolites have shown remarkable activity for selective partial oxidation of methane³¹⁻³⁸. Geometric constraints and confinement effects by zeolite microporous structures result in enhanced activity of α -oxygen of ferryl iron ($[\text{Fe}=\text{O}]^{2+}$) active center, showing a low C-H activation barrier for methane (≤ 0.3 eV)^{33-35,37}. However, the strong hydrophilicity of zeolite frameworks leads to strongly bound reaction product (methanol) inside the pores, limiting activity to relatively high temperature regime (≥ 200 °C)^{32,37,38}. This limitation might be overcome by using metal organic frameworks (MOFs), which are highly tunable microporous solid materials. However, currently Fe-loaded MOFs seem to be far from low-temperature applications: Fe(II) loaded on MOF-74 is unstable for long time^{39,40}, Fe(II) on some MIL families requires overwhelmingly high oxidation energy⁴¹, and Fe(III) on MIL-53 suffers from very low loading limitations⁴².

Recently, single Fe-atom catalyst stabilized by N atoms on graphene carbon nanosheet (FeN_4/GN) was reported to be active for the selective CH_4 conversion to C_1 products with a very low CO_2 selectivity (6 % for 10 hr.)⁴³. The authors showed that H_2O_2 oxidizes the Fe site to form active oxygenated sites that can convert CH_4 into CH_3OOH or CH_3OH , which can be further oxidized to HCOOH or HOCH_2OOH ⁴³. The energy barrier for the first C-H cleavage was so small that the reaction could proceed even at ambient temperature, avoiding over-oxidation⁴³. This catalytic system is remarkably promising in that a non-precious metal (Fe) shows high activity and remains stable even longer than the other coordinatively-unsaturated metal systems because of the highly stable C-N bonds in N-doped graphene⁴⁴. Furthermore, the graphene support is advantageous because not only it allows high dispersion of the stabilized FeN_4 centers, but also its carbon network enhances the catalytic activity of the active site^{43,44}.

Herein, driven by the aforementioned experimental discoveries we conduct a detailed computational study for methane activation and conversion on the FeN_4/GN catalyst. We specifically focus on obtaining a mechanistic understanding of methane-to-methanol conversion in the presence of the oxidant, H_2O_2 , by investigating a series of possible reactions. We also consider solvent effects (water) to account for experimental conditions and report estimated turnover frequencies (TOFs) addressing the overall reactivity of the catalyst. Our results reveal the nature of the active center and provide an in-depth mechanistic understanding of methanol synthesis from methane. Overall, this work can further guide efforts on the discovery of energy efficient methods for methane conversion to liquids.

Computational Details

Density functional theory (DFT) calculations were performed with the Gaussian 09 software package at the B3LYP/6-31G(d) level of theory⁴⁵⁻⁴⁷. Benchmark calculations validate that the level of theory chosen can accurately capture the reported

catalytic trends (see supporting information). All the geometries at local minima or saddle points were fully optimized and verified with the mode and number of imaginary vibrational frequencies (transition state has one and ground state does not have an imaginary frequency). Furthermore, intrinsic reaction coordinate (IRC) calculations⁴⁸ were carried out for the optimized transition states (TS) to confirm that they accurately connect the corresponding reactants and products. The catalyst system is composed of central single Fe atom and 4 N atoms, surrounded by 26 C atoms with the graphene edges terminated by H atoms (Figure S1). In the lowest energy spin state (triplet) of the system, the C-C bond lengths vary between 1.37-1.43 Å, which is close to that of pure graphene (1.42 Å). The Fe-N bond length is 1.895 Å, which is consistent with previous reports^{49,50}. The Gibbs free energies of the elementary oxidation/hydroxylation reactions of the Fe site for the formation of active sites were calculated from eqn. (1) and (2):

$$G_{\text{oxi}} = (G_{\text{cat-O}} + G_{\text{H}_2\text{O}}) - (G_{\text{cat}} + G_{\text{H}_2\text{O}_2}) \quad (1)$$

$$G_{\text{hydroxy}} = G_{\text{cat-OH}} - \left(G_{\text{cat}} + \frac{1}{2} G_{\text{H}_2\text{O}_2} \right) \quad (2)$$

where G_{cat} stands for the Gibbs free energy of the catalyst before reaction, and $G_{\text{cat-O}}$ and $G_{\text{cat-OH}}$ are those of the catalysts obtained one oxygen and hydroxyl on the Fe site, respectively. Also, $G_{\text{H}_2\text{O}}$ and $G_{\text{H}_2\text{O}_2}$ represent the Gibbs free energies of H_2O and H_2O_2 molecules, respectively. The energy changes along the reaction pathways were described in terms of Gibbs free energy. Through all the Gibbs free energy calculations, enthalpy and entropy corrections were applied to the electronic energy assuming 1 atm and 298.15 K. Solvent effects were taken into consideration applying the conductor-like polarizable continuum model (CPCM)⁵¹ using water as the solvent, since the reaction experimentally takes place in the presence of water⁴³. Turn over frequencies (TOFs) of different pathways were calculated based on the energetic span model of S. Kozuch and S. Shaik⁵² at room temperature.

Results and Discussion

1. Active site formation

The FeN_4 center embedded on the graphene structure can be oxidized by the oxidant (H_2O_2), forming highly reactive oxygen sites⁴³, as well as hydroxyl sites. To understand the active site nature, we calculated the oxidation and hydroxylation energies of the catalyst at the ground spin state as shown in Figure 1. The detailed profiles of the active center formation under various spin states are presented in the Supporting Information (Figure S2). Both the first oxidation and hydroxylation steps from the bare FeN_4/GN are exothermic, where the former is energetically more favorable. The second oxidation from the mono-oxo species is endothermic, while hydroxylation is slightly exothermic forming hydroxy(oxo) center. The formation of the hydroxy(oxo) species is the most preferred among all considered (-1.77 eV), followed by the mono-oxo center (-1.71 eV). Two consecutive hydroxylation reactions result in di-

hydroxy center, which is also stable with a formation energy of -1.57 eV.

2. Methane-to-methanol conversion mechanisms

(1) Di-oxo FeN₄/GN

Even though our calculations demonstrate that the mono-oxo FeN₄/GN structure is more favorable than the di-oxo one, the latter is considered first as Deng et al.⁴⁴ suggested that the Fe site exists in a symmetrical O=Fe=O structure. We investigated three different mechanisms of methane-to-methanol conversion on the triplet di-oxo structure as shown in Figure 2 and S3. The di-oxo centers in triplet and quintet spin states are isoenergetic (Figure S2), but we confirmed that an intersystem crossing (ISC) will not alter the energetics in all pathways presented, since there were no transition states that were lower in energy in the high spin state (i.e. quintet). All mechanisms are radical-based as the first step is a homolytic C-H bond cleavage through a H abstraction by the reactive O, resulting in the formation of a free methyl radical and a hydroxyl ligand (TS 1). The H abstraction has been regarded as a key concept of methane activation by transition metal oxide cations/complexes and enzymes. The energy required for the C-H cleavage step is 0.67 eV, which is comparable to relevant methane activation barriers that have been reported in literature (i.e., homolytic C-H cleavage that involves free methyl radical formation): 0.76 eV on Fe-O modified graphene⁵³, 0.72 - 0.99 eV on Fe-ZSM-5^{54,55}, 0.72 eV on Fe-loaded MOF-74³⁹, and 0.64 - 0.79 on Fe-loaded MIL families^{41,42}. The generated methyl radical, in turn, produces CH₃OH via reaction with hydroxyl (called "oxygen rebound process"), which was suggested to occur on heme iron containing enzymes (cytochrome P-450) and non-heme iron center of soluble methane monooxygenase^{25,56-58}. This step has very small reaction barrier (0.14 eV, TS 2). Thereafter, CH₃OH is desorbed to leave the Fe site exposed to H₂O₂, which regenerates the oxo center (TS 3) and completes the catalytic cycle. Even though the cleavage of the strong C-H bond (which normally limits the methane activation) is facile (0.67 eV, TS 1), the whole cycle is limited by

the energy-demanding O recovery step (1.24 eV, TS 3). In other words, the active site regeneration appears to govern the activity of the di-oxo FeN₄/GN catalyst for the methane conversion through path 1a.

Mechanistically, there is no difference between path 1a and the pathway suggested to occur on the single non-heme Fe center stabilized on several MOF families⁴¹. However, the di-oxo FeN₄/GN is more active than these MOFs since the latter require higher energy input to regenerate the active site from N₂O oxidant (1.24 eV, TS 3 vs. 1.45 eV), even though the C-H activation is energetically similar (0.67 eV, TS 1 vs. 0.62 eV)⁴¹. The di-iron complexes on Fe-ZSM-5 were also reported to homolytically dissociate the C-H bond of methane, but these intrinsically complicated systems involve multiple mechanisms to produce methanol⁵⁵. On the other hand, the single Fe site in the Fe-ZSM-5 catalyzes methane in a different pathway³⁶: a hydroxymethyl (HO-Fe-CH₃) center is formed through a single C-H dissociation step, which in turn, produces methanol via recombination of methyl and hydroxyl. This mechanism is essentially similar to how metal oxide cations ([MO]⁺) catalyze methane as suggested by Yoshizawa et al.^{26,27} The hydroxymethyl intermediate can also be generated on the iron-oxo centers of the FeN₄/GN catalysts. This non-radical type C-H dissociation, however, does not occur in the ground spin state (triplet). Furthermore, the activation energies of this C-H activation were found to be 2.89 and 2.35 eV on the mono-oxo and di-oxo centers, respectively (results not shown). Therefore, the pathways that involve the hydroxymethyl intermediate are ruled out in this study.

Since H₂O₂ is used as an oxidant, this energetically demanding active site recovery step (TS 3) can be bypassed. In an alternative pathway (path 1b, Figure 2(b)), after the first C-H cleavage, the produced methyl radical can react with a H₂O₂ molecule (from the liquid phase) to produce CH₃OH and a hydroxyl radical with a small activation energy (0.60 eV, TS 4). The remaining hydroxyl radical attacks the H of the hydroxyl ligand on Fe, regenerating the active O site with a negligible reaction barrier (0.02 eV, TS 5). As a H₂O₂ molecule participates in the middle of the pathway rather than simply recovering the active site as in path 1a, this pathway is characterized as H₂O₂-mediated. Considering that the highest energy barrier in the whole cycle is only 0.67 eV for the C-H activation (TS 1), this pathway is energetically plausible, plus, there is an exothermic adsorption of H₂O₂ from the liquid phase (step 22) compared to path 1a. Nevertheless, the two identified transition states to produce methanol, i.e., TS 2 in path 1a and TS 4 in path 1b, are competing as the reactants are essentially the same except for the additional H₂O₂ molecule in 22. Therefore, the ratio of intermediates (19 vs. 23) can be determined by the difference in the activation energies in accordance with the Curtin-Hammett principle^{59,60}. From the commonly shared intermediate (18), the energy barriers for TS 2 and TS 4 are 0.14 and 0.37 eV respectively, which give the dominant population of intermediate 19 ($6.74\text{E}3$ times more than intermediate 23). In other words, most of the di-oxo centers will end up being in a mono-oxo form (3) as being trapped by the demanding active site recovery step (TS 3) instead of completing the cycle. This

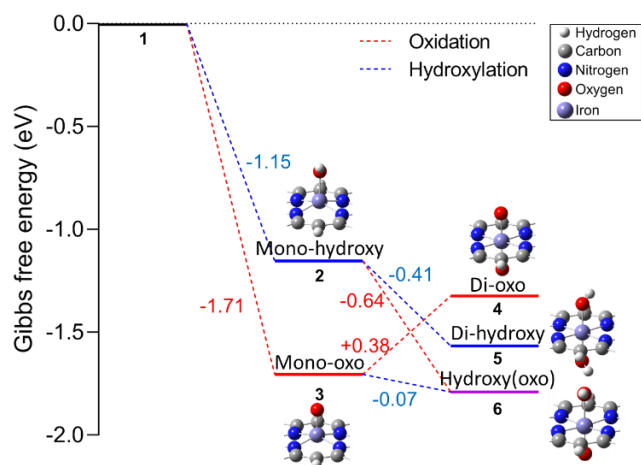


Figure 1. Free energy profiles of formation of various active centers by oxidation/hydroxylation on the Fe center of the FeN₄/GN system.

leads to the investigation of the mono-oxo center mechanisms, which will be presented in the following section.

Additionally, one more pathway on the di-oxo center is found as given in the Supporting Information (path 1c, Figure S3), where the produced methyl radical is stabilized by one of N atoms surrounding the Fe center. Due to the larger reaction barriers (0.75 eV, TS 6 and 1.34 eV, TS 7), however, this pathway is less likely to occur than path 1a and b. Also, a pathway with a singlet di-oxo FeN₄/GN (energetically unfavorable spin state) was investigated for comparison, which can be found in the Supporting Information (path2, Figure S4).

(2) Mono-oxo FeN₄/GN

As presented in Figure 1 and S2, our DFT calculations indicate the mono-oxo FeN₄/GN in the triplet spin state to be the second most stable form of the catalyst. This is in contrast to computational results reported by Deng et al.⁴⁴, where the di-oxo structure was energetically more stable than the mono-oxo. It should be noted that the thermodynamic preference of the mono-oxo over the di-oxo state, reported in Figure S2, can be further supported from an oxidation state perspective. The oxidation state of Fe at the FeN₄ center embedded in six-membered rings (or pyridinic FeN₄ site) is +2^{49,50}. This, in turn, increases to +4 and +6 forming mono-oxo (Fe=O) and di-oxo (O=Fe=O) centers respectively. Despite the presence of Fe(VI) species in the highly oxidized form (e.g., FeO₄²⁻)⁶¹, this high oxidation state is relatively uncommon compared to the Fe(IV)-oxo complexes⁶². This ferryl moiety (Fe(IV)=O), in fact, has been identified as the active site of heme-containing monooxygenases (cytochrome P-450)^{56,57} and Fe-ZSM-5³⁴ for hydrocarbon activation. Finally, our mechanistic scenario in the previous subsection indicates that the di-oxo center will eventually be converted to the mono-oxo form, which is the thermodynamically most stable between the two forms. Under this consideration, we investigated the methane-to-methanol conversion mechanisms on the mono-oxo FeN₄/GN.

It becomes apparent that all reaction mechanisms considered in the di-oxo FeN₄/GN catalyst (Figure 2 and S3) can take place on the mono-oxo as the single O-site exists in both cases. The equivalent pathways to path 1a and b are presented as path 3a and b in Figure 3 (the counterpart of path 1c was not investigated due to the high TS energies involved). The activation energy for the first C-H cleavage from methane (1.58 eV, TS 10) is more than twice as high as that found on the di-oxo catalyst (0.67 eV, TS 1). The activation energy is lower than the value reported by T. Roongcharoen et al. (1.91 eV)⁶³, but both values are consistently high so that the O site on the mono-oxo catalyst is inactive under ambient temperature. This lower activity comes from the lower basicity of the active site, compared to that of the di-oxo center. The H affinity^{64,65} or H binding energy⁶⁶⁻⁶⁸ has been reported to be a descriptor for the hydrocarbon activation via homolytic C-H bond cleavage. Here, we calculated the H atom binding energy (BE_H) from eqn. (3) and related it to the activation energy for the homolytic C-H cleavage (ΔG_{C-H}) on all the active centers presented in Figure 1. The BE_H and ΔG_{C-H} (Figure 4) show a clear scaling relation,

confirming the BE_H as a good descriptor for methane activation via homolytic C-H bond cleavage. This indicates that the O site on the mono-oxo catalyst has low activity because of its low basicity, while that of the di-oxo catalyst is a relatively strong base resulting in the facile C-H cleavage. Furthermore, we found a strong relationship between the oxidation state of the Fe centers and basicity of the active sites, in such a way that the basicity increases with the oxidation number of Fe from +3 (mono-hydroxy) to +6 (di-oxo). Notably, the mono-oxo and di-hydroxy centers form the same Fe(IV) oxidation state and have almost same BE_H of ~ -0.8 eV. The two different active sites of the hydroxy(oxo) center (Fe(V)) also show close basicity. These results reveal an interesting observation: the homolytic C-H dissociation of methane by the oxo or hydroxy active sites on

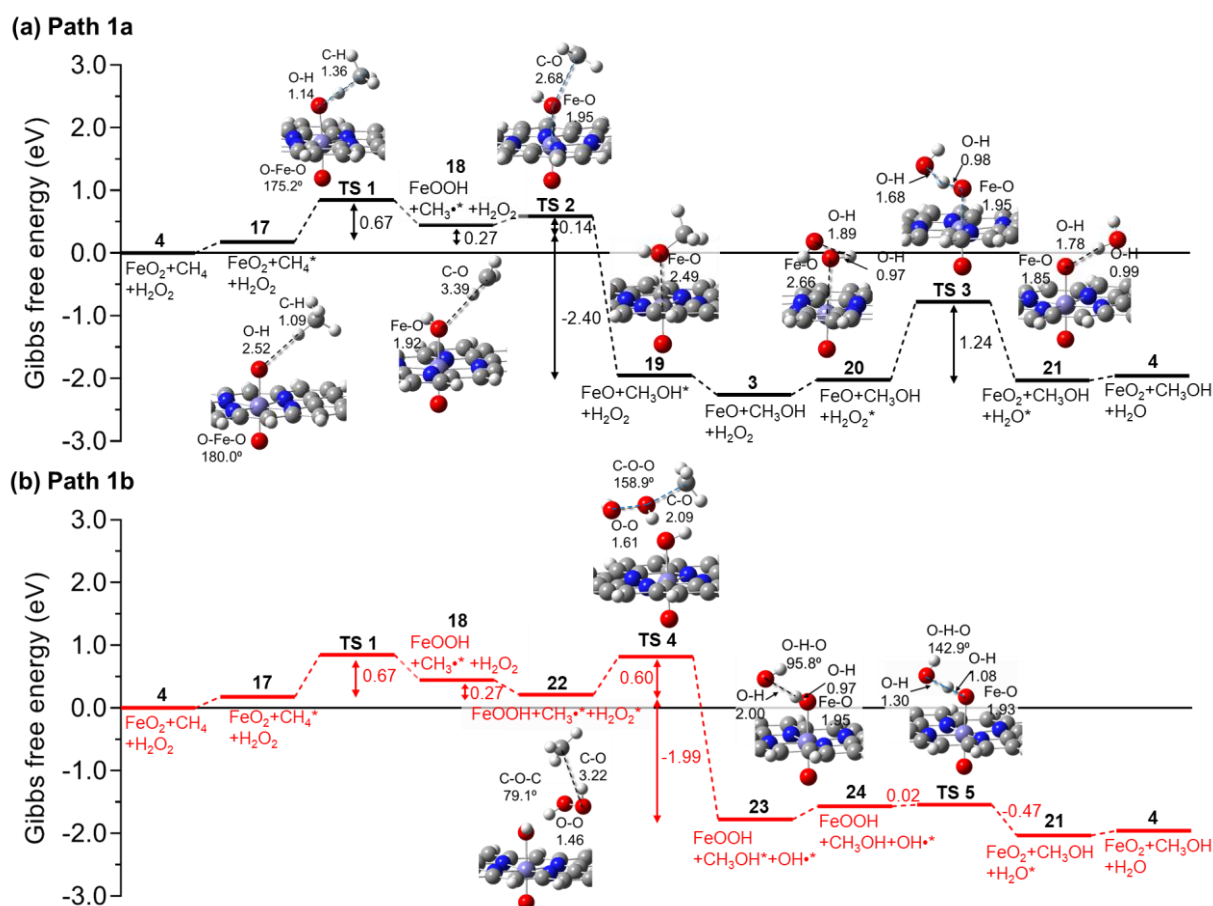


Figure 2. Detailed free energy profiles of methane conversion to methanol by the di-oxo FeN_4/GN catalyst (triplet state) following (a) path 1a and (b) path 1b. “Fe” on the profiles stands for FeN_4/GN catalyst structure, and “TS” represents a transition state. Asterisk (*) denotes adsorbed species on the catalyst surface. The first four steps are identical in both pathways. Select interatomic distances (in Å) are shown on the molecular structures.

the FeN_4/GN catalyst is modulated by the oxidation state of Fe, rather than a type of the active site.

$$BE_H = G_{(\text{cat}-\text{H})} - G_{(\text{cat})} - \frac{1}{2}G_{(\text{H}_2(\text{g}))} \quad (3)$$

Interestingly, the methane activation can potentially occur not only directly by O but also indirectly by Fe, which is exposed to the reactants at the non-oxidized side of the mono-oxo structure. Unlike the path 3a and b, this mechanism is initiated by the H_2O_2 adsorption rather than C-H activation (path 4, Figure 3(c)). A H_2O_2 molecule is adsorbed on the center in such a way that the one hydroxyl is closely bound to Fe while the other one is facing outwards. Overcoming a relatively small energy barrier (0.64 eV, TS 15), a hydroxyl radical is formed, simultaneously hydroxylating the Fe center. In turn, the produced hydroxyl radical abstracts H from CH_4 to generate water and methyl radical (TS 16). Due to the highly active nature of the hydroxyl radical, the activation barrier for the homolytic C-H cleavage is only 0.35 eV. After water desorption, the methyl radical reacts with the remaining hydroxyl ligand to produce CH_3OH . The highest barrier corresponds to the O-O bond dissociation of H_2O_2 for OH radical generation at only 0.64 eV (TS 15). Indeed, it is known that CH_4 can be catalyzed into its

oxygenates under mild conditions with the presence of H_2O_2 and O_2 , where transition metals generate hydroxyl radicals from H_2O_2 , and the radicals abstract H from CH_4 to produce methyl radicals⁶⁹⁻⁷¹; this is known as Fenton-type reaction⁷². This type of C-H activation has also been previously suggested to occur with a small barrier (0.77 eV) on Fe-ZSM-5 catalyst⁵⁵. Specifically, the authors reported that the dissociation of O-O bond of H_2O_2 and methane activation via the C-H cleavage took place in a single step⁵⁵. Considering that methyl hydroperoxide (CH_3OOH), which is one of the major products from the Fenton-type methane oxidation⁵⁵, was experimentally observed in large quantity⁴³, the Fenton mechanisms seem plausible. However, Hammond et al.⁷³ reported that the mechanism of methane conversion to methanol with H_2O_2 by Cu-promoted Fe-ZSM-5 was different from the Fenton-type reaction. Further considering the complicated nature of the Fenton chemistry^{74,75}, this highlights the challenge on elucidating radical chemistries.

It is worth noting that the structure obtained after the water desorption on path 4 (18 in Figure 3(c)) was already found on path 1a-c (on the di-oxo catalyst). This shows that, instead of going through TS 2 as suggested in path 3, the produced methyl radical can react with H_2O_2 generating CH_3OH and OH radical, steps which are found in path 1b (steps 22-TS 4-23). If this

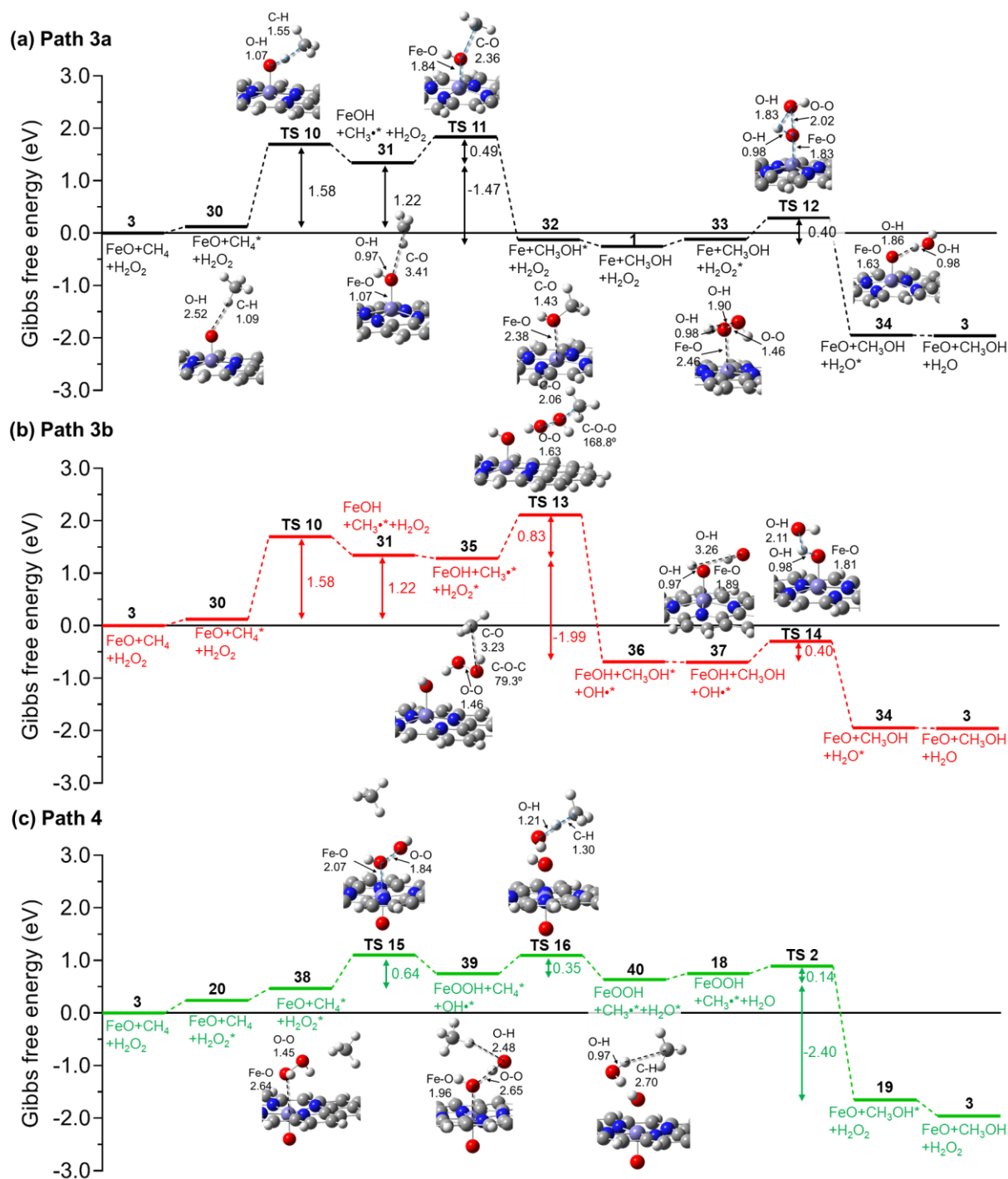


Figure 3. Detailed free energy profiles of methane conversion to methanol by the mono-oxo FeN_4/GN catalyst (triplet state) following (a) path 3a, (b) path 3b, and (c) path 4. Select interatomic distances (in Å) are shown on the molecular structures.

occurs, the mono-oxo center will be converted to the di-oxo configuration by being oxidized rather than acting as a catalyst, which indicates the possibility of a dynamic oxidation behavior of the Fe center. However, as also pointed out in the previous section, our statistical analysis based on the Boltzmann probability shows that this is not likely to occur. As shown in Figure 1, the free energy of the mono-oxo is lower than that of the di-oxo by 0.30 eV, and this leads to the dominant population of the mono-oxo over di-oxo at 298.15 K. In an alternative

partway, the methyl radical can also be stabilized by N (as TS 6 in path 1c), but this pathway will be energetically demanding.

(3) Hydroxy(oxo) FeN_4/GN

Both the oxygen and hydroxyl active sites on the hydroxy(oxo) FeN_4/GN catalyst are shown to have a high activation energy for the initial C-H cleavage (around 1.2 eV) as presented in Figure 4. Nonetheless, the bifunctional hydroxy(oxo) center may play an important role as one of the key species, because it is the most

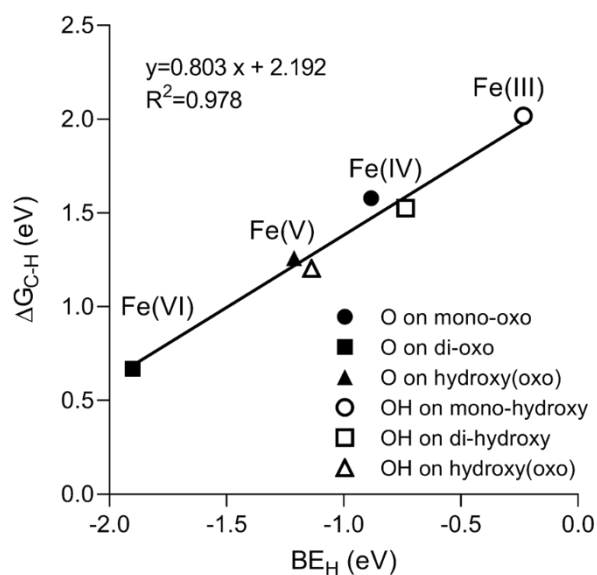


Figure 4. Linear relationship between the H binding energy (BE_H) and the energy barrier for the homolytic C-H cleavage of methane (ΔG_{C-H}). The oxidation states of each Fe center are displayed along the data points.

stable form of the catalyst (Figure 1) and seems to appear in the middle of reactions on oxo-catalysts along with adsorbed radical species (intermediate 18 in path 1a and 4, and intermediate 23 in path 1b). Therefore, the mechanisms of methane-to-methanol conversion by the hydroxy(oxo) center are studied in detail. The catalysts in ground spin (doublet) and high spin (quartet) states are isoenergetic (Figure S2), and we found ISC may occur in one pathway as discussed below.

All the pathways found on the di-oxo center can take place on the oxo site of the hydroxy(oxo) center: path 5a and b in Figure 5 correspond to path 1a and b (Figure 2), respectively (the counterpart of path 1c is not studied). Mechanistically, the only difference is that the hydroxyl radical produced by the reaction between methyl radical and H_2O_2 in path 5b abstracts hydrogen from the hydroxylated center without any barrier (steps 47-45). Comparing the energetics, however, the hydroxy(oxo) center is distinctly different from the di-oxo center. Due to the low basicity of the active O site, the C-H activation is more demanding ($\Delta G_a = 1.27$ eV, TS 17), but the activation barrier for the regeneration of the active site from a H_2O_2 molecule is significantly decreased (1.24 eV, TS 3, path 1a \rightarrow 0.73 eV, TS 19, path 5a). Furthermore, as shown in Figure S2, the mono-hydroxy center (13) is more stable in the quartet spin state, which indicates that the system may involve ISC between doublet and quartet spin states through TS 18, although the activation barrier of TS 18 is higher in quartet. In the high spin state, the active site recover step is more facile (TS 19, $\Delta G_a = 0.43$ eV; note that this reported value can only be obtained with partial optimization relevant to the transition state). In turn, the facile active site recovery eliminates the advantage of the H_2O_2 -mediated mechanism (path 5b) over path 5a. The hydroxyl site of the hydroxy(oxo) center can also be an active site; another H_2O_2 -mediated mechanism is identified as shown in Figure S5 in

the Supporting Information (path 5c). However, except that the methanol production and active site recovery occur simultaneously (TS 22), path 5c is essentially same to path 5b not only mechanistically but energetically, and thus the detailed description is omitted. Lastly, a concerted mechanism is found on the oxo site (path 5d, Figure S5), which corresponds to path 2 on the singlet di-oxo center. The high activation barrier (1.76 eV, TS 23) makes the pathway unlikely.

3. Solvent effects

In order to demonstrate how the water solvent affects the reaction mechanisms, the CPCM⁵¹ was applied on the important pathways found on the di-oxo (path 1a and b) and mono-oxo (path 4) FeN_4/GN catalysts, as shown in Figures S6. Solvent effects on the other pathways were not investigated because of their unfavorable energetics. Overall, the presence of the solvent does not modify the reaction mechanism, although the energetics of the elementary steps are affected. On the di-oxo center, the water desorption becomes exothermic (steps 21-4), because the polar water molecule is not favored to be adsorbed on the catalyst in the presence of the solvent. Likewise, desorption of a produced CH_3OH on path 1b becomes more facile (steps 23-24). The remaining adsorption/desorption steps are practically unchanged. Importantly, all the reaction barriers in path 1a and b decrease except for TS 2, which is still small although having doubled in the presence of water (0.14 eV \rightarrow 0.27 eV, TS 2). As a result, the methane-to-methanol conversion on the di-oxo center becomes more facile in the presence of water solvent. Nevertheless, the barrier for the O recovery is reduced slightly by 1.6 % (1.24 eV \rightarrow 1.22 eV, TS 3) so that path 1a is still demanding in comparison to path 1b. It is worth noting that the change of the energetics alters the ratio of intermediates 19 vs. 23: from the shared state 18, the barrier for TS 2 is doubled while that for TS 4 is only slightly increased (by 0.07 eV) as solvent effects are considered. As a result, the population ratio of 19 to 23 is reduced by one order of magnitude (6.74E3 on gas phase \rightarrow 6.87E2 under water solvation), which means the contribution of path 1b to the overall activity increases, albeit it remains still small. In case of path 4 on the mono-oxo center, the energy barrier for C-H cleavage by OH radical is decreased under the presence of the solvent (0.35 eV \rightarrow 0.28 eV, TS 16). However, the rate-

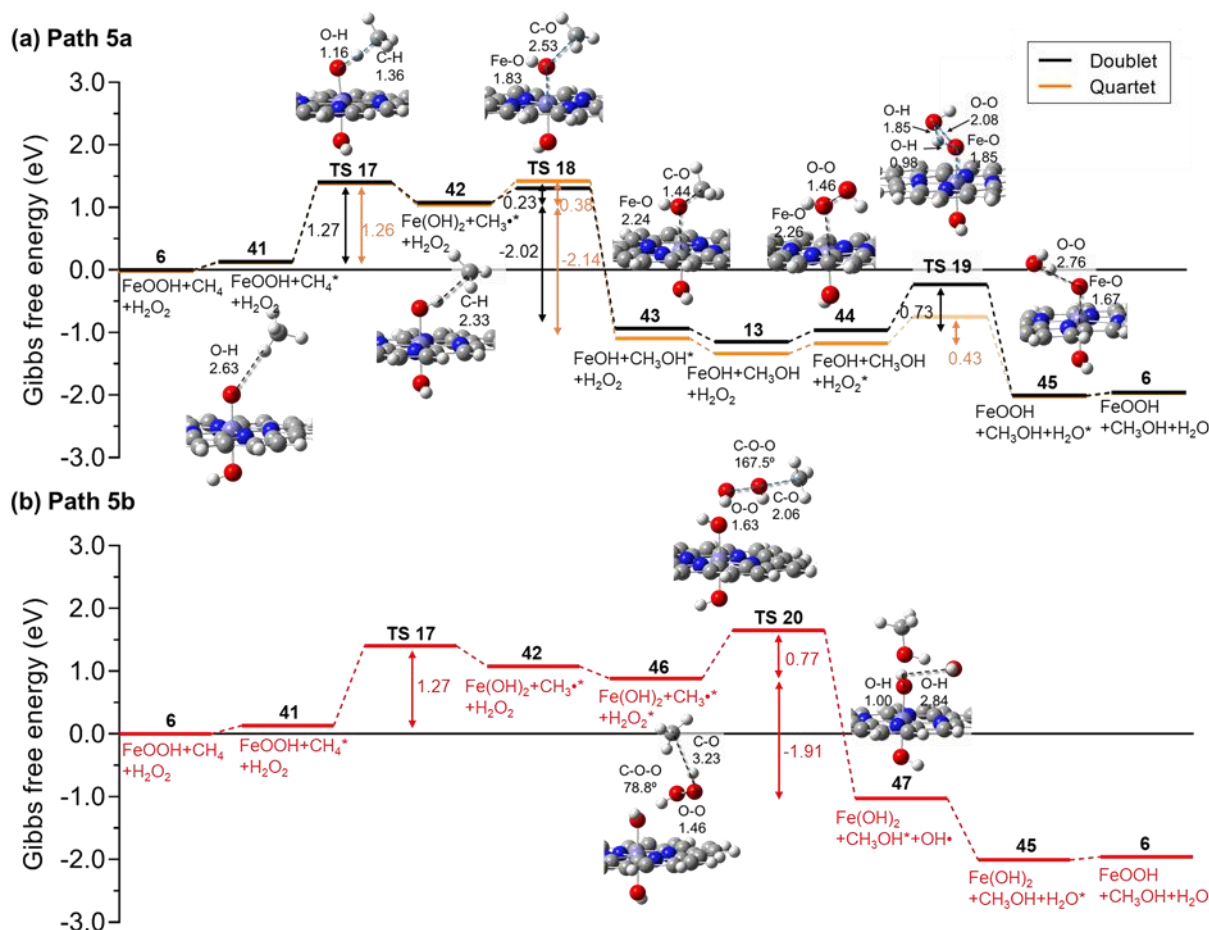


Figure 5. Detailed free energy profiles of methane conversion to methanol by the hydroxy-oxo FeN_4/GN catalyst (doublet state) following (a) path 5a and (b) path 5b. The energy profile of path 5a at the high spin state (quartet) is also presented in panel (a) in orange. The TS 19 in quartet could not be located and the energy value was obtained with partial optimization. Select interatomic distances (in Å) are shown on the molecular structures. In panel (a), only doublet structures are presented.

determining OH radical generation becomes less facile as the energy barrier increases ($0.64 \text{ eV} \rightarrow 0.76 \text{ eV}$, TS 15). Hence, the catalytic activity of the mono-oxo FeN_4/GN appears to decrease when considering solvent effects.

4. Energetic span model

Although the detailed reaction energy profiles presented so far provide quantitative information for each elementary step, they cannot rationalize the overall reaction pathway activity. The energetic span model provides accurate estimates of TOF for a given catalytic cycle based on its detailed energetics⁵². Thus, we calculated the TOFs of all the cycles investigated in this work as tabulated in Table 1. As expected, path 1a and c show poor TOFs because of the large energy barriers involved. On the other hand, the TOF of path 1b is higher than those of path 1a and c by more than 9 orders of magnitude in the gas phase, and increases by 80 times in the presence of solvent. This result clearly demonstrates that path 1b is the most efficient catalytic cycle on the di-oxo FeN_4/GN . Again, it must be noted that the results do not indicate that the di-oxo center is highly active, since path 1a is favored over 1b based on the Curtin-Hammett principle as discussed above. In case of the mono-oxo center, the high energy barrier for the homolytic C-H cleavage limits the

TOFs of path 3a and b at very low levels, but path 4 turns out to be very efficient, even more than path 1b. However, the calculated TOF of path 4 significantly decreases in the presence of water by more than 200 times, because of the increased barrier for the OH radical generation step (TS 15). The TOFs of the pathways on the singlet di-oxo and hydroxy(oxo) catalysts are extremely low as expected, so that they would not contribute to catalyzing the methanol synthesis reaction. As discussed, the path 5a on the hydroxy(oxo) center may involve ISC between low (doublet) and high (quartet) spin states. However, the probable ISC does not affect the TOF because the energy span of the pathway is essentially identical. Overall, in the gas-phase, the mono-oxo catalyst is the most active configuration as path 4 exhibits the largest TOF ($1.60\text{E}-2 \text{ s}^{-1}$), followed by the di-oxo center (path 1b, TOF: $1.49\text{E}-3 \text{ s}^{-1}$). On the other hand, in the presence of a solvated environment, the TOF of path 4 in mono-oxo center decreases by more than 200 times (TOF: $7.16\text{E}-5 \text{ s}^{-1}$), while that of path 1b in di-oxo center increases to be the most efficient pathway (TOF: $1.12\text{E}-1 \text{ s}^{-1}$). However, the population dominance of the mono-oxo center over the di-oxo is still valid in the presence of water based on the Boltzmann statistics, as the mono-oxo center is thermodynamically more favorable than the di-oxo. This

suggests that the overall TOF is expected to be mostly contributed by the mono-oxo center. Combining these observations together, the solvated environment can unfavorably affect the overall catalytic efficiency. It is worth noting that the most active pathways among all (i.e., path 1b and 4) spend H_2O_2 as a reactant, rather than limiting its role for the active oxygen regeneration as reported in previous studies^{43,44}: H_2O_2 can directly react with methyl radical to produce CH_3OH (path 1b – H_2O_2 -mediated mechanism), or be activated by the Fe center to form OH radical, which can abstract H from CH_4 (path 4 – Fenton-type mechanism). This observation emphasizes the importance of the role of the oxidant in this specific reaction network.

Table 1. Calculated turn over frequencies (TOFs) of the investigated pathways based on the energetic span model⁵². The pathways investigated applying the CPCM solvation model⁵¹ are denoted as “sol”.

| Catalyst | Pathway | TOF (s^{-1}) |
|------------------|-------------|-------------------------|
| Di-oxo | Path 1a | 4.85E-13 |
| | Path 1a-sol | 7.19E-13 |
| | Path 1b | 1.49E-3 |
| | Path 1b-sol | 1.12E-1 |
| | Path 1c | 3.51E-15 |
| Di-oxo (singlet) | Path 2 | 8.54E-13 |
| Mono-oxo | Path 3a | 9.65E-19 |
| | Path 3b | 2.19E-23 |
| | Path 4 | 1.60E-2 |
| | Path 4-sol | 7.16E-5 |
| Hydroxy(oxo) | Path 5a | 1.88E-12 |
| | Path 5b | 1.23E-16 |
| | Path 5c | 1.50E-19 |
| | Path 5d | 1.13E-20 |

Conclusions

In this work, we applied DFT calculations to investigate in detail the mechanisms of methane conversion to methanol using H_2O_2 on the single Fe-atom catalyst stabilized by N-functionalized graphene nanosheet (FeN_4/GN). Our results demonstrated that iron-oxo centers (mono-oxo and di-oxo) generated under reaction conditions can readily catalyze CH_4 even under ambient temperatures, whereas, the hydroxylated state of the catalyst is inert. By taking into consideration a number of different reaction pathways, catalyst configurations, and solvent effects, we revealed that reactive O-sites on the di-oxo catalyst are able to efficiently abstract H from CH_4 to generate methyl radical (methane activation), which can further react with either the hydroxylated center or the oxidant H_2O_2 . As the reaction involves the energetically demanding O-site regeneration, however, the di-oxo catalyst is likely to be converted to the mono-oxo form. Compared to the di-oxo, the mono-oxo catalyst is thermodynamically more stable under reaction conditions, but the most active site appears to be the

Fe center and not the oxygen site of the catalyst. The oxygen site is found to be inactive due to its low basicity, which stems from the oxidation state of Fe center (+4). In contrast, the Fe center can catalyze methane to methanol through a Fenton-type mechanism by first dissociating the O-O bond of H_2O_2 to produce OH radical, which in turn easily activates CH_4 and converts it to methanol. We revealed that the most feasible pathway on the mono-oxo catalysts consume the oxidant H_2O_2 as a reactant, not limiting its role to the active site regeneration as previously suggested. Solvent effects (presence of water) can either accelerate or slow down the methanol synthesis reaction depending on the mechanism and active center. However, considering the thermodynamic dominance of the mono-oxo centers and the mechanisms that take place on these centers, the presence of water solvent appears to reduce the overall catalytic activity. Taken together, our computational work sheds light into a very complex interplay between thermodynamics of active site formation, competition of different reaction mechanisms and solvent effects for the methane-to-methanol conversion on FeN_4/GN catalyst. Our findings can potentially guide experimental efforts to discover efficient catalysts converting methane to liquids at ambient conditions. Especially, our investigation regarding the solvation effects can be extended further to the processes that involve a gas-phase oxidant instead of H_2O_2 , e.g., N_2O^{41} , O_3^{76} , and O_2^{58} , since such systems, depending on the operation conditions, can also be in a solvation environment of a polar liquid products (such as methanol). Future computational work in this area may include 1) the exploration of possible ligands that can block one face of the iron center in order to prevent the formation of the inactive hydroxyl site; 2) the introduction of explicit water molecules for more accurate investigation of water solvation effects; and 3) the use of microkinetic modelling for better understanding the complicated catalytic mechanisms.

Author Contributions

G. M. conceived the project and S. H. performed all the calculations of this work. Both authors have contributed to the preparation of the manuscript.

Conflicts of interest

There are no conflicts to declare.

Acknowledgements

This work was supported by the National Science Foundation (NSF), under grant no. 1920623 and by the Central Research Development Funds (CRDF) of the University of Pittsburgh. The authors would like to acknowledge computational support from the Center for Research Computing at the University of Pittsburgh.

References

1. International energy outlook 2019 with projections to 2050, <https://www.eia.gov/outlooks/ieo/pdf/ieo2019.pdf>, (accessed October 2020).
2. S.-Y. Lee and G. D. Holder, *Fuel processing technology*, 2001, **71**, 181-186.
3. J. B. Curtis, *AAPG bulletin*, 2002, **86**, 1921-1938.
4. K. C. Surendra, D. Takara, A. G. Hashimoto and S. K. Khanal, *Renewable and Sustainable Energy Reviews*, 2014, **31**, 846-859.
5. N. D. Parkyns, C. I. Warburton and J. D. Wilson, *Catalysis Today*, 1993, **18**, 385-442.
6. C. Sayin, *Fuel*, 2010, **89**, 3410-3415.
7. S. Wasmus and A. Küver, *Journal of Electroanalytical Chemistry*, 1999, **461**, 14-31.
8. M. Stöcker, *Microporous and Mesoporous Materials*, 1999, **29**, 3-48.
9. U. Olsbye, S. Svelle, M. Bjørgen, P. Beato, T. V. W. Janssens, F. Joensen, S. Bordiga and K. P. Lillerud, *Angewandte Chemie International Edition*, 2012, **51**, 5810-5831.
10. P. Tian, Y. Wei, M. Ye and Z. Liu, *Acs Catalysis*, 2015, **5**, 1922-1938.
11. A. P. York, T. Xiao and M. L. Green, *Topics in Catalysis*, 2003, **22**, 345-358.
12. H. D. Gesser, N. R. Hunter and C. B. Prakash, *Chemical Reviews*, 1985, **85**, 235-244.
13. J. R. Rostrup-Nielsen, J. Sehested and J. K. Nørskov, *Advances in catalysis*, 2002, **47**, 65-139.
14. N. J. Gunsalus, A. Koppaka, S. H. Park, S. M. Bischof, B. G. Hashiguchi and R. A. Periana, *Chemical reviews*, 2017, **117**, 8521-8573.
15. R. Horn and R. Schlögl, *Catalysis Letters*, 2015, **145**, 23-39.
16. R. H. Crabtree, *Chemical Reviews*, 1995, **95**, 987-1007.
17. M. M. Kappes and R. H. Staley, *Journal of the American Chemical Society*, 1981, **103**, 1286-1287.
18. M. M. Kappes and R. H. Staley, *The Journal of Physical Chemistry*, 1981, **85**, 942-944.
19. B. S. Freiser, *Talanta*, 1985, **32**, 697-708.
20. T. C. Jackson, T. J. Carlin and B. S. Freiser, *Journal of the American Chemical Society*, 1986, **108**, 1120-1126.
21. S. K. Loh, E. R. Fisher, L. Lian, R. H. Schulz and P. B. Armentrout, *Journal of Physical Chemistry*, 1989, **93**, 3159-3167.
22. D. E. Clemmer, Y.-M. Chen, F. A. Khan and P. B. Armentrout, *The Journal of Physical Chemistry*, 1994, **98**, 6522-6529.
23. D. Schröder and H. Schwarz, *Angewandte Chemie International Edition*, 1990, **29**, 1433-1434.
24. A. Fiedler, D. Schroeder, S. Shaik and H. Schwarz, *Journal of the American Chemical Society*, 1994, **116**, 10734-10741.
25. D. Schröder and H. Schwarz, *Angewandte Chemie International Edition*, 1995, **34**, 1973-1995.
26. K. Yoshizawa, Y. Shiota and T. Yamabe, *Chemistry—A European Journal*, 1997, **3**, 1160-1169.
27. K. Yoshizawa, Y. Shiota and T. Yamabe, *Journal of the American Chemical Society*, 1998, **120**, 564-572.
28. K. Yoshizawa, Y. Shiota and T. Yamabe, *The Journal of Chemical Physics*, 1999, **111**, 538-545.
29. V. I. Sobolev, K. A. Dubkov, O. V. Panna and G. I. Panov, *Catalysis Today*, 1995, **24**, 251-252.
30. G. I. Panov, V. I. Sobolev, K. A. Dubkov and A. S. Kharitonov, *Studies in Surface Science and Catalysis*, 1996, **101**, 493-502.
31. A. Zecchina, M. Rivallan, G. Berlier, C. Lamberti and G. Ricchiardi, *Physical Chemistry Chemical Physics*, 2007, **9**, 3483-3499.
32. M. V. Parfenov, E. V. Starokon, L. V. Pirutko and G. I. Panov, *Journal of Catalysis*, 2014, **318**, 14-21.
33. A. Rosa, G. Ricchiardi and E. J. Baerends, *Inorganic Chemistry*, 2010, **49**, 3866-3880.
34. B. E. Snyder, P. Vanelderen, M. L. Bols, S. D. Hallaert, L. H. Böttger, L. Ungur, K. Pierloot, R. A. Schoonheydt, B. F. Sels and E. I. Solomon, *Nature*, 2016, **536**, 317-321.
35. F. Goltl, C. Michel, P. C. Andrikopoulos, A. M. Love, J. Hafner, I. Hermans and P. Sautet, *ACS Catalysis*, 2016, **6**, 8404-8409.
36. M. H. Mahyuddin, A. Staykov, Y. Shiota and K. Yoshizawa, *ACS Catalysis*, 2016, **6**, 8321-8331.
37. M. H. Mahyuddin, Y. Shiota, A. Staykov and K. Yoshizawa, *Inorganic Chemistry*, 2017, **56**, 10370-10380.
38. P. Sazama, J. Moravkova, S. Sklenak, A. Vondrova, E. Tabor, G. Sadovska and R. Pilar, *ACS Catalysis*, 2020, **10**, 3984-4002.
39. P. Verma, K. D. Vogiatzis, N. Planas, J. Borycz, D. J. Xiao, J. R. Long, L. Gagliardi and D. G. Truhlar, *Journal of the American Chemical Society*, 2015, **137**, 5770-5781.
40. D. J. Xiao, E. D. Bloch, J. A. Mason, W. L. Queen, M. R. Hudson, N. Planas, J. Borycz, A. L. Dzubak, P. Verma and K. Lee, *Nature Chemistry*, 2014, **6**, 590-595.
41. J. G. Vitillo, A. Bhan, C. J. Cramer, C. C. Lu and L. Gagliardi, *ACS Catalysis*, 2019, **9**, 2870-2879.
42. D. Y. Osadchii, A. I. Olivos-Suarez, Á. Szécsényi, G. Li, M. A. Nasalevich, I. A. Dugulan, P. S. Crespo, E. J. Hensen, S. L. Veber and M. V. Fedin, *ACS Catalysis*, 2018, **8**, 5542-5548.
43. X. Cui, H. Li, Y. Wang, Y. Hu, L. Hua, H. Li, X. Han, Q. Liu, F. Yang and L. He, *Chem*, 2018, **4**, 1902-1910.
44. D. Deng, X. Chen, L. Yu, X. Wu, Q. Liu, Y. Liu, H. Yang, H. Tian, Y. Hu and P. Du, *Science advances*, 2015, **1**, e1500462.
45. M. J. Frisch, G. W. Trucks, H. B. Schlegel, G. E. Scuseria, M. A. Robb, J. R. Cheeseman, G. Scalmani, V. Barone, B. Mennucci, G. A. Petersson, H. Nakatsuji, M. Caricato, X. Li, H. P. Hratchian, A. F. Izmaylov, J. Bloino, G. Zheng, J. L. Sonnenberg, M. Hada, M. Ehara, K. Toyota, R. Fukuda, J. Hasegawa, M. Ishida, T. Nakajima, Y. Honda, O. Kitao, H. Nakai, T. Vreven, J. A. M. Jr., J. E. Peralta, F. Ogliaro, M. Bearpark, J. J. Heyd, E. Brothers, K. N. Kudin, V. N. Staroverov, R. Kobayashi, J. Normand, K. Raghavachari, A. Rendell, J. C. Burant, S. S. Iyengar, J. Tomasi, M. Cossi, N. Rega, J. M. Millam, M. Klene, J. E. Knox, J. B. Cross, V. Bakken, C. Adamo, J. Jaramillo, R. Gomperts, R. E. Stratmann, O. Yazyev, A. J. Austin, R. Cammi, C. Pomelli, J. W. Ochterski, R. L. Martin, K. Morokuma, V. G. Zakrzewski, G. A. Voth, P. Salvador, J. J. Dannenberg, S. Dapprich, A. D. Daniels, O. Farkas, J. B. Foresman, J. V. Ortiz, J. Cioslowski and D. J. Fox, GAUSSIAN 09 (Revision D.01), Gaussian Inc., Wallingford, CT, 2014.
46. A. D. Becke, *The Journal of chemical physics*, 1992, **96**, 2155-2160.
47. C. Lee, W. Yang and R. G. Parr, *Physical review B*, 1988, **37**, 785.
48. C. Gonzalez and H. B. Schlegel, *The Journal of Chemical Physics*, 1989, **90**, 2154-2161.
49. A. N. Andriotis, G. Mpourmpakis, S. Broderick, K. Rajan, S. Datta, M. Sunkara and M. Menon, *The Journal of Chemical Physics*, 2014, **140**, 094705.

50. A. Titov, P. Zapol, P. Král, D.-J. Liu, H. Iddir, K. Baishya and L. A. Curtiss, *The Journal of Physical Chemistry C*, 2009, **113**, 21629-21634.
51. V. Barone and M. Cossi, *The Journal of Physical Chemistry A*, 1998, **102**, 1995-2001.
52. S. Kozuch and S. Shaik, *Accounts of Chemical Research*, 2011, **44**, 101-110.
53. S. Impeng, P. Khongpracha, C. Warakulwit, B. Jansang, J. Sirijaraensre, M. Ehara and J. Limtrakul, *RSC Advances*, 2014, **4**, 12572-12578.
54. W. Liang, A. T. Bell, M. Head-Gordon and A. K. Chakraborty, *The Journal of Physical Chemistry B*, 2004, **108**, 4362-4368.
55. Á. Szécsényi, G. Li, J. Gascon and E. A. Pidko, *ACS Catalysis*, 2018, **8**, 7961-7972.
56. J. T. Groves, 1985, **62**, 928-931.
57. V. W. Bowry and K. U. Ingold, *Journal of the American Chemical Society*, 1991, **113**, 5699-5707.
58. P. C. Wilkins, H. Dalton, I. D. Podmore, N. Deighton and M. C. R. Symons, *European Journal of Biochemistry*, 1992, **210**, 67-72.
59. D. Y. Curtin, *Record of Chemical Progress*, 1954, **15**, 110-128.
60. J. I. Seeman, *Chemical Reviews*, 1983, **83**, 83-134.
61. H. Goff and R. K. Murmann, *Journal of the American Chemical Society*, 1971, **93**, 6058-6065.
62. E. V. Rybak-Akimova, in *Physical Inorganic Chemistry Reactions, Processes and Applications*, ed. A. Bakac, Wiley, Hoboken, NJ, 2010, Mechanisms of oxygen binding and activation at transition metal centers, pp. 109-188.
63. T. Roongcharoen, S. Impeng, N. Kungwan and S. Namuangruk, *Applied Surface Science*, 2020, **527**, 146833.
64. A. A. Latimer, A. R. Kulkarni, H. Aljama, J. H. Montoya, J. S. Yoo, C. Tsai, F. Abild-Pedersen, F. Studt and J. K. Nørskov, *Nature Materials*, 2017, **16**, 225-229.
65. E. C. Tyo, C. Yin, M. Di Vece, Q. Qian, G. Kwon, S. Lee, B. Lee, J. E. DeBartolo, S. Seifert and R. E. Winans, *ACS Catalysis*, 2012, **2**, 2409-2423.
66. H. Aljama, J. K. Nørskov and F. Abild-Pedersen, *The Journal of Physical Chemistry C*, 2017, **121**, 16440-16446.
67. M. Dixit, P. Kostetsky and G. Mpourmpakis, *ACS Catalysis*, 2018, **8**, 11570-11578.
68. M. C. Cholewinski, M. Dixit and G. Mpourmpakis, *ACS Omega*, 2018, **3**, 18242-18250.
69. G. B. Shulpin and G. V. Nizova, *Reaction Kinetics and Catalysis Letters*, 1992, **48**, 333-338.
70. G. V. Nizova, G. Süß-Fink and G. B. Shul'pin, *Chemical Communications*, 1997, 397-398.
71. G. Süß-Fink, G. V. Nizova, S. Stanislas and G. B. Shul'pin, *Journal of Molecular Catalysis A: Chemical*, 1998, **130**, 163-170.
72. C. C. Winterbourn, *Toxicology Letters*, 1995, **82**, 969-974.
73. C. Hammond, M. M. Forde, M. H. Ab Rahim, A. Thetford, Q. He, R. L. Jenkins, N. Dimitratos, J. A. Lopez-Sanchez, N. F. Dummer and D. M. Murphy, *Angewandte Chemie*, 2012, **124**, 5219-5223.
74. B. Ensing, F. Buda and E. J. Baerends, *The Journal of Physical Chemistry A*, 2003, **107**, 5722-5731.
75. A. S. Petit, R. C. R. Penniford and J. N. Harvey, *Inorganic Chemistry*, 2014, **53**, 6473-6481.
76. A. Božović, S. Feil, G. K. Koyanagi, A. A. Viggiano, X. Zhang, M. Schlagen, H. Schwarz and D. K. Bohme, *Chemistry—A European Journal*, 2010, **16**, 11605-11610.